INVESTIGATION OF THE VERY HIGH CYCLE FATIGUE BEHAVIOUR OF GFRP CROSS-PLY BENDING SPECIMENS

T.J. Adam*, P. Horst

*Institute of Aircraft Design and Lightweight Structures, Technische Universität Braunschweig, 38108 Braunschweig, Germany, *tj.adam@tu-braunschweig.de*

Keywords: Very high cycle fatigue, polymer composites, damage mechanisms

Abstract

High frequency bending fatigue experiments are conducted to investigate damage mechanisms, their interaction and stiffness degradation of GFRP flat specimens at very high cycle numbers. By using a special VHCF test rig and testing at frequencies between 50 Hz and 80 Hz the so called very high cycle fatigue range is reached within a reasonable amount of time. Online stiffness measurement and transmitted light photography are used for damage monitoring. First data is presented for a $[90/0]_s$ cross-ply laminate. Crack densities and delaminated area fractions are determined and used for numerical calculation of stiffness decrease. Stiffness degradation and modulus calculation is scrutinized by means of numerical and quasi static experiments.

1. Introduction

As fatigue of fibre-reinforced plastics (FRP) is a complex issue, it has been one of the main focuses in world-wide composite research since the 1960s. So far, a broad base of knowledge concerning the mechanisms of fatigue, their interaction as well as numerous theoretical modeling approaches has been established. However, experimental experience is mostly limited to the high cycle fatigue range (HCF, 1×10^6 cycles), rarely exceeding 1×10^7 cycles. This lack of knowledge beyond HCF usually leads to rather conservative designs. Even though there are numerous applications reaching the so-called very high cycle fatigue (VHCF) range (e.g. GFRP wind turbine rotor blades due to service times of up to 30 years or light-weight CFRP compressor blades of aero engines due to frequency), the very high cycle fatigue behavior of FRP has not been sufficiently investigated yet [1].

1.1. Available studies on VHCF of composite materials

An early series of tests investigating the long-term fatigue of typical wind turbine materials has been conducted by Mandell *et al.* in the 1990s. Most of the tests conducted under the auspices of the U.S. Department of Energy (DOE) were constant-amplitude (SN) tests of flat cupons. A high-speed procedure allowing tests at up to 100 Hz was developed [2-4]. These comprehensive tests mainly comprise SN data not investigating underlying mechanisms. More recent VHCF studies examining the effect of stress level on the growth rates of transversal matrix cracks and delamination have been published by Hosoi *et al.* [5-9]. It is found that a tensile load amplitude below 30 % of the static failure stress shifts final specimen rupture into the VHCF range. Furthermore, a change in the order of appearance of transversal cracks and delamination is observed. Neither matrix cracking nor delamination can be found

at stress amplitudes smaller than 20 % of the static strength. Hosoi *et al.* reveal that the change in fatigue damage growth behavior is caused by different growth rates of cracking and delamination at each stress level.

1.2 Challenges of VHCF testing and recent approach

All approaches to VHCF trying to shorten testing times by raising frequency have to cope with specimen overheating. Usually, this is overcome by limiting specimen thickness (Mandell *et al.*: $t = 1.5\,mm$ and fibre strands, Hosoi *et al.*: $t = 1.1\,mm$). Further problems are the measurement of stress parameters by means of strain gauges or extensometers and the self-fatigue of standard servo-hydraulic testing machines. In fact, even running tests with durations of several weeks is a delicate matter and requires robust and in best case specifically designed equipment. In order to circumvent typical problems, a special test rig has been developed [10-11]. Its basic idea is that the heat transfer problem within the specimens can be solved by simply not stressing all laminate sections equally. This means, that *bending*, which mainly stresses exterior layers, is an adequate load case for VHCF-testing. Furthermore, it allows the specific investigation of thin laminas bonded to a carrying, non-degrading core laminate. The recent experimental approach provides short testing times by testing at elevated frequencies between 50 Hz and 80 Hz. Several online damage monitoring techniques are used to investigate degradation behavior, damage mechanisms and phenomenology at VHCF loads. First experimental results for a $[90/0]_s$ GFRP laminate will be presented. Additionally, basic observations and underlying assumptions will be verified by means of numerical and quasi-static tests.

2. Experimental Methods and Testing Equipment

2.1. VHCF Bending Test Rig and Damage Monitoring

A special test rig for high frequent VHCF four-point bending has been set up. Its main asset is that testing times are shortened by testing at frequencies between 50 Hz and 80 Hz while specimen temperature does not increase more than 10°C above room temperature. Due to the four-point-bending (Fig. 1), a large area of uniform damage growth located in the region of constant maximum bending moment can be investigated.

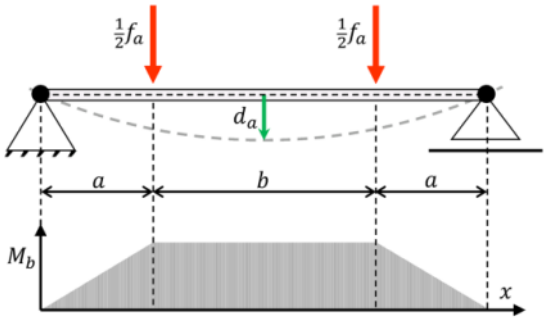

Figure 1. Geometric parameters of four point bending test, $a = 20\,mm, b = 40\,mm$, amplitudes of force f_a and deflection d_a

An overview of the test rig imbedding four bending platforms is depicted in Figure 2. Each platform is an independent bending test as depicted in Fig. 2 B. It is driven by a customized electro dynamic actuator allowing frequencies of up to *80* Hz (non-resonant), depending on the specimen configuration. A flat bending specimen (t = *2* mm, w = *25* mm, l = *82* mm) is embedded in a two-sided light-weight four-point bending device (R = *-1*). Eight rotatable

low-friction trunnions (four on each side of the specimen) prevent frictional heating and abrasive damage of the specimen. With the middle part of the device deflected by a light-weight actuator rod, a sinusoidal bending load is applied. Both parameters load (one load f on each side of the device) and maximum deflection d_a are measured online by means of two load cells and a triangulation laser. The measurement of load and deflection is used for two purposes. Firstly, for controlling load or deflection by means of a control circuit in *Lab View*®. Secondly, for calculating the dynamic secant bending modulus in terms of damage monitoring. Furthermore, two optical techniques, thermography and transmitted light photography, have been integrated into the test rig. Especially transmitted light photography, which is based on a flat cold light lamp in the moving part of the bending device, provides detailed images of matrix cracking and delamination in transparent or opaque GFRP materials. All monitoring techniques are online techniques. Thus, there are no undesired effects due to removing the specimen for characterization throughout the test. Another aspect is the control of ambient temperature. As bending forces are relatively small (30 N ≤ f_a ≤ 500 N) and as most light-weight devices are made of aluminum, changes in ambient temperature have undesired effects. Therefore, the rig is housed in an air-conditioned chamber with a temperature of 20 ± 1.5 °C.

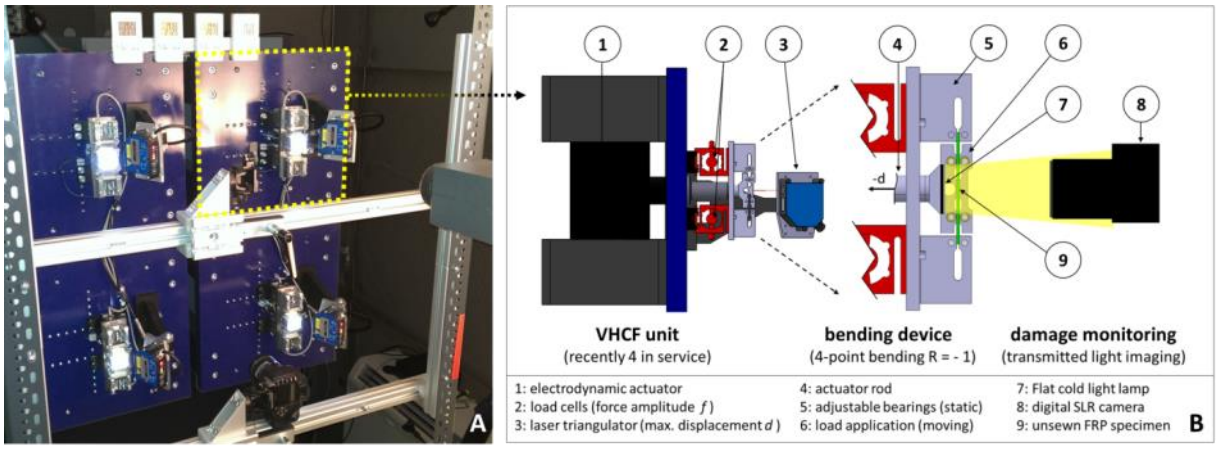

Figure 2. Overview of theVHCF test rig with four bending units (A), concept of the bending device (B)

2.2. Damage Evaluation

Fatigue damage is evaluated in two different ways, by calculating the loss in bending stiffness continuously throughout the test and by the determination of crack densities and delaminated area. The specimens' effective bending (secant) modulus $\bar{E}_{xb}$ is calculated by means of the 4-point bending equation and the geometric parameters given in Fig. 1.

$$\bar{E}_{x\mathrm{b}} = \frac{f_\mathrm{a}}{d_\mathrm{a}} \frac{6}{wt^3} \left(\frac{1}{3}a^3 + \frac{1}{2}ba^2 + \frac{1}{8}ab^2 \right) \tag{1}$$

The bar implies a simplification concerning the calculation of the elastic modulus of the damaged specimen. For an undamaged specimen, $\bar{E}_{xb}$ can be determined from the maximum bending deflection and force. However, with the fatigue damage decreasing towards both ends of the specimen, this approach does not reflect the stiffness loss of the uniformly damaged central region accurately. For this reason, the implied error has been assessed by means of quasi-static experiments and analytical considerations. It has been found that the influence of the undamaged specimen regions is small and that the simplified bending

modulus $\bar{E}_{x\mathrm{b}}$ only deviates slightly from $E_{x\mathrm{b}}$. Figure 3 depicts the predicted error of the $\bar{E}_{x\mathrm{b}}$ determination method. The error has been predicted by means of an analytical first order four-point bending beam model with changing elastic moduli in longitudinal direction. In this model, damage (stiffness degradation) growing towards the specimen ends (sections a in Fig. 1) is assumed to be equal to region b degradation. As specimen damage typically takes course around the designated path, the error of $\bar{E}_{x\mathrm{b}}$ determination is expected to be small.

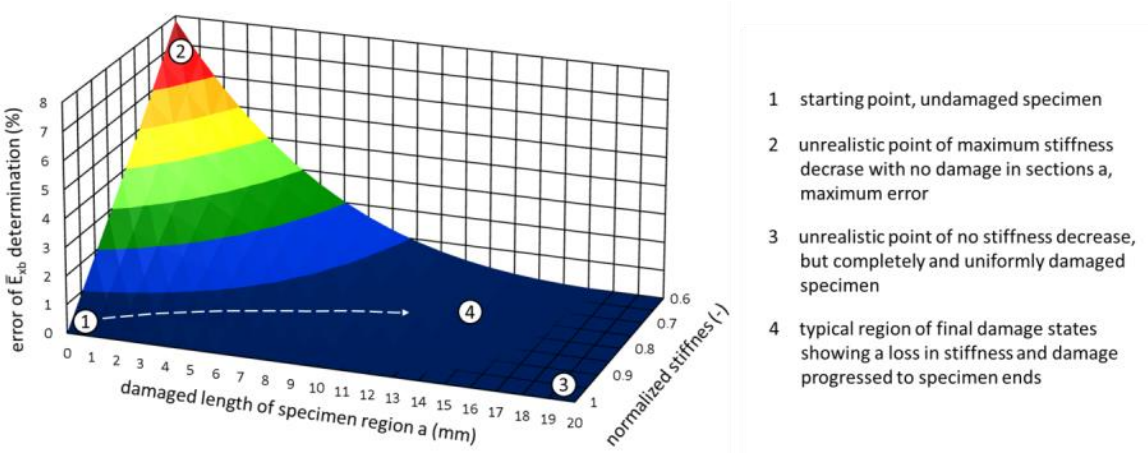

Figure 3. Theoretical Error of $\bar{E}_{x\mathrm{b}}$ determination, predicted analytically by means of first order four-point-bending beam with subdivided moduli in longitudinal direction

A more accurate experimental method would be to additionally measure the displacement of the inner rollers and to substract it from the maximum displacement. As this approach requires the use of a second laser triangulator per platform and thus increases the complexity of the whole high frequency measuring system, the simplification seems to be passable.

Concerning the optical monitoring, an average transverse crack density of the constantly stressed middle part of the specimen is calculated by the sum of all crack lengths per window area. As cracks grow equally in both sides of the specimen ($R = -1$) and as this cannot be differentiated in the transmitted light pictures, crack length is divided by two.

$$\rho_{90^\circ} = \frac{\sum_{i=0}^{n} l_{crack,i}}{2 \cdot l_{window} \cdot w_{specimen}} \tag{2}$$

Furthermore, the total debonded area A_{delam}, which is measured by means of digital image analysis is used to calculate the delaminated area fraction.

$$daf_{90^\circ} = \frac{A_{\mathrm{delam}}}{2 \cdot l_{window} \cdot w_{specimen}} \tag{3}$$

2.3. Quasi-static bending tests

A series of standard quasi-static four-point bending tests has been conducted to generate reference data on stiffness decrease due to transverse cracking. Thereby, transverse cracking has been induced using the VHCF bending configuration (*a = 20* mm, *b = 40* mm, *L = 80* mm) depicted in Figure 1. Then, after each step of damage creation the effective bending stiffness has been determined using a bending configuration matching the specimen center part (*a = 10*, *b = 20* mm, *L = 40* mm).

2.4 Numerical and analytical calculation of stiffness degradation

A one dimensional shear-lag approach presented by Smith *et al.* [12] as well as a FEM based Representative Surface Element (RSE, FEM) of a cracked cross-ply laminate are used for validating the experimental stiffness degradation data. In contrast to Schmitz *et al.* [13] using a complex 3d unit cell to determine bending stiffness matrices of cracked heterogeneous materials, a simplified 2d model limited to E_{xb} calculation is used in the present study.

3. Specimen Preparation

All specimens tested in cyclic and quasi-static experiments are $[90/0]_s$ GFRP flat specimen with a laminate thickness of 2 mm and four single-layers of 0.5 mm. As sewing threads are imperfections causing inner heating (at higher frequencies) and given that they affect the crack and delamination observation as well, the laminate is produced unsewn by CNC roving stacking and RTM. The constituents are glass fibre rovings Owens Corning OC111AX (1200 tex) and a cold curing epoxy system Momentive RIM135/RIMH137. The average fibre volume fraction is 0.40. After cutting to specimen size, edges are polished to remove micro cracks.

4. Experimental Results and Discussion

3.1. Results of VHCF Tests

So far, experimental data has been gained for a GFRP cross-ply $[90/0]_s$ which has been tested at a frequency of 50 Hz. Tests have been conducted at three different load levels, each starting at an initial deflection with an initial maximum surface strain $\varepsilon_{22,0}^{90^\circ}$ and a corresponding stress of $\sigma_{22,0}^{90^\circ}$ in the transverse direction of the 90°-plies (see Table 1. for analytical values). The strategy behind was to lower the load from one load level to the next to investigate changes in fatigue behavior – from HFC to VHCF.

Load Level	$\boldsymbol{\varepsilon_{22,0}^{90^\circ}}$ **/ %**	$\boldsymbol{\sigma_{22,0}^{90^\circ}}$ **/ MPa**
LL1	0.44	39
LL2	0.37	33
LL3	0.26	23

Table 1. Load Levels for load controlled VHCF tests

As known from the HCF range, transverse cracking and delamination are the major damage mechanisms in cross-ply layups – under axial loads as well as for bending. An exemplary transmitted light picture of the constantly stressed middle part of a specimen is depicted in Fig. 4 A. Concerning the transverse cracks, it is observed that they mainly initiate at the free edges. After initiation, they grow across the specimen width and the ply thickness. Through-the-thickness crack growth is an essential difference between axial and bending load cases and is found to be crucial for interlaminar damage. Delamination is the second mechanism which in all cases initiates after transverse cracking has progressed. However, no edge delamination occurs at all. 90°/0°-interface delamination areas are initiated locally when transverse cracks growing in through-the-thickness direction are stopped by the 0°-layer. After initiation, the growth of transverse cracking and delamination causes bending stiffness to decrease. The extent of fatigue damage and stiffness decrease depends on the load level as known from literature. As it is a matter of common knowledge, lowering the stress amplitude shifts stiffness degradation and final failure to higher cycle numbers.

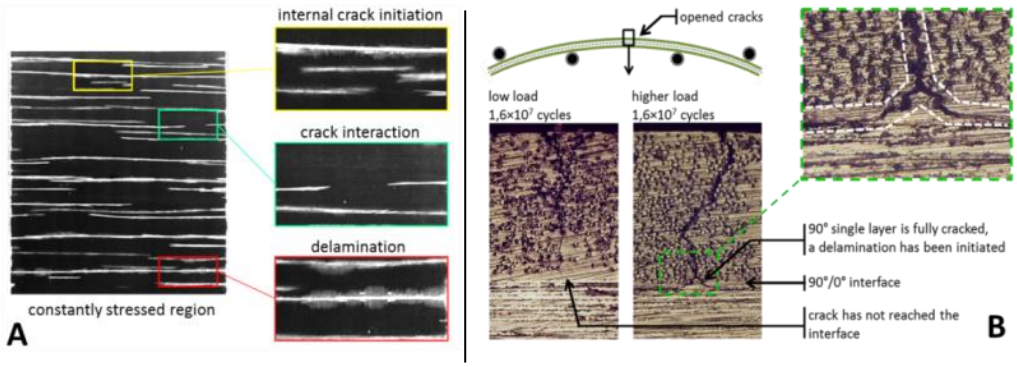

Figure 4. Transmitted light picture of typical damage phenomenoms (A) and edge-micrograph showing transverse through-the-thickness cracking (B)

Fig. 5 depicts the results of damage monitoring – the normalized bending modulus, the transverse crack density and the fraction of delaminated area plotted against cycle numbers. All three diagrams illustrate the effect of load level. Whereas stiffness degradation and transverse cracking starts immediately at LL1 and LL2 leading to crack saturation and final stiffness within the first 1×10^6 cycles, both are delayed in the case of LL3.

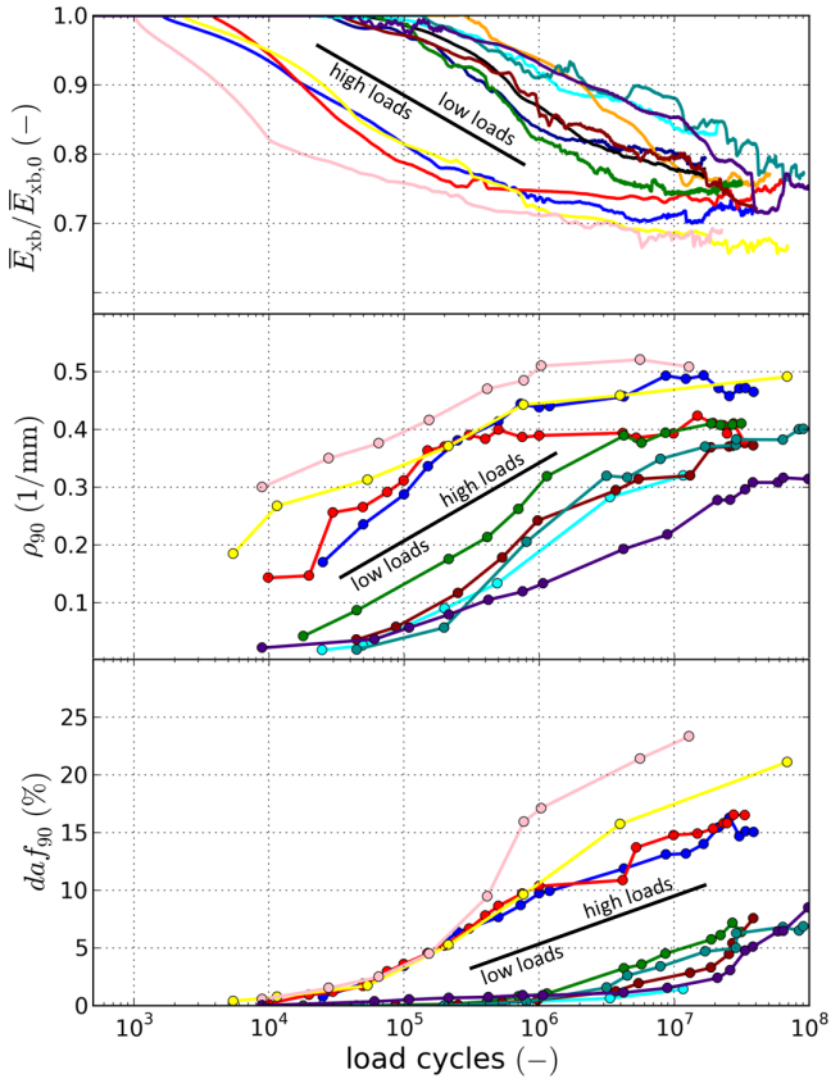

Figure 5. Normalized bending stiffness, transverse crack density and delaminated area fraction of all load levels LL1-LL3 against log scaled load cycles up to 10^8

Here, crack densities increase rather slowly approaching saturation in the range between 1×10^7 to 2×10^7 cycles. Stiffness degradation behaves similarly. It becomes obvious that saturation crack densities are higher for LL1 and LL2 and accordingly, stiffness decreases to lower values. Regarding delamination, the difference between high and low loads is even more distinct. LL1 and LL2 lead to an early initiation and growth of delamination and area fractions greater than 15 % of the constantly stressed middle part of the specimen. Noticeably, delamination occurs before transverse cracking has saturated. In contrast, delamination is delayed and of minor occurrence at the lower load level. Maximum values beyond 3×10^7cycles stay below 10 %. It is obvious that slower through-the-thickness crack growth leads to delayed delamination initiation. Then, at an advanced cracking state, delamination progresses more slowly. Delamination fraction still increases after crack saturation has been reached. One further observation is that none of the specimens tested reach final rupture, not even those tested at the highest stress level. As damage growth slows down significantly after the point of crack saturation, experiments have been stopped after a while. The nonappearance of final failure presumably results from the laminate configuration. With the 90°-layers being fully degraded and the middle 0°-layers bearing the load, the specimens become very flexible. However, as the resulting maximum strain in the 0°-layers is small, the onset of damage is probably a timely matter. None of the specimens tested showed the onset of longitudinal cracking even at 1×10^8 cycles.

4.2 Results of quasi-static tests, FEM and shear-lag theory

As stiffness only depends on the amount of damage, but not on the way it has been induced (cyclic or quasi-static), quasi-static tests are used to verify stiffness degradation detected in the VHCF tests. Figure 6 A correlates stiffness degradation with crack density for all VHCF load levels. A rather linear damage-degradation relation with good agreement for all load levels can be seen. Figure 6 B compares a linear fit of this data with results from static four-point bending tests (S4PB), a one dimensional shear-lag approach and a simple FEM based representative surface element (2D-RSE) of the cracked laminate. All results are in good agreement in the range of low crack densities. At crack densities $\rho_{90°} > 0.3\ 1/\text{mm}$ the theoretical graphs flatten towards ply discount, whereas the fatigue data shows a further linear decrease. This behavior results from delamination which is neither existent under quasi-static loading nor considered in FEM and the shear-lag model. All in all, the experimental fatigue stiffness degradation data is represented well.

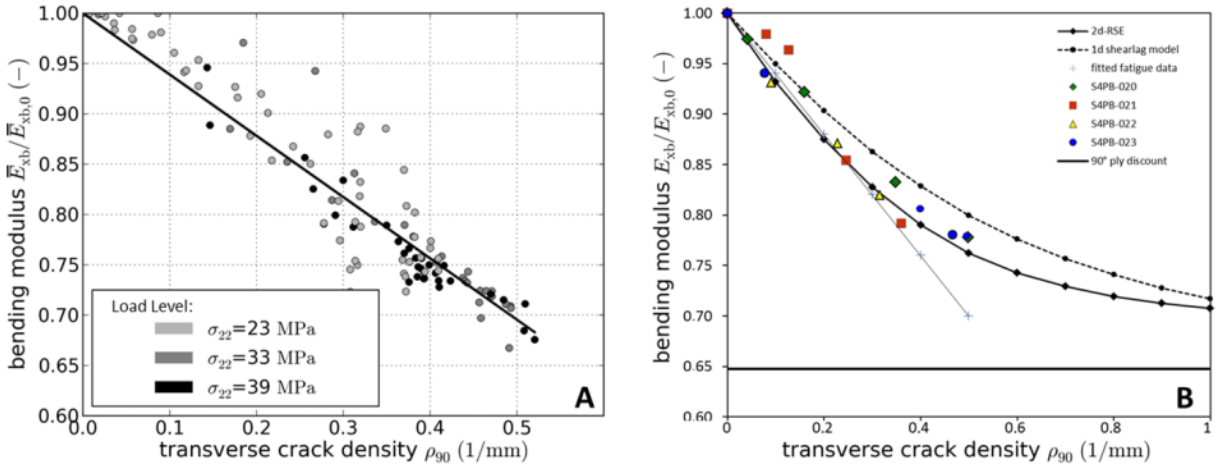

Figure 6. Stiffness degradation against crack density for all load levels tested in the VHCF tests (A), comparison of the fitted fatigue data with results from static four-point bending tests (S4PB), numerical data of a representative surface element (2D-RSE) and analytical values from 1D shear-lag approach (B)

5. Conclusion

A series of $[90/0]_s$ GFRP cross-ply specimen has been tested up to 10^8 load cycles by means of a specialized high frequency four-point bending fatigue test rig. Stiffness degradation, transverse cracking and delamination are monitored with online techniques. Then, damage parameters (crack densities and delaminated area fractions) are calculated to investigate the effect of load level and the fatigue process at low loads. Low loads extend degradation beyond 10^7 cycles. Delamination is delayed by slower through-the-thickness crack growth. Stiffness loss has been verified by means of a shear-lag approach and FEM. Besides the load dependent changes in cracking- and delamination behavior, no unexpected mechanisms have been found. Further tests will be conducted at even lower loads to identify a threshold for crack initiation.

Acknowledgements

The work has been founded by the German Research Foundation (DFG) within the Priority Program 1466.

References

[1] C. Bathias. An engineering point of view about fatigue of polymer matrix composite materials", *International Journal of Fatigue*, 28, pp. 1094-1099, 2006
[2] J.F. Mandell, R.M. Reed, D.D. Samborsky, Q. Pan. Fatigue performance of wind turbine blade composite materials, *SED-Vol. 14, Wind Energy*, ASME, 1993
[3] J.F. Mandell, D.D. Samborsky. DOE/MSU composite material fatigue database: test methods, materials and analysis, *Contractor Report*, SAND97-3002, 1997
[4] J.F. Mandell, D.D Samborsky, L. Wang. New fatigue data for wind turbine blade materials, *AIAA-2003-0692*, Montana State University, 2003
[5] Hosoi, N. Sato, Y. Kusumoto, K. Fujiwara, H. Kawada. High-cycle fatigue characteristics of quasi-isotropic cfrp laminates over 10^8 cycles (Initiation and propagation of delamination considering interaction with transverse cracks), *Int. Journal of Fatigue*, 32, pp. 29-36, 2010
[6] Hosoi, K. Takamura, N. Sato, H. Kawada. Quantitative evaluation of fatigue damage growth in cfrp laminates that changes due to applied stress level, *Int. Journal of Fatigue*, 33, pp. 781-787, 2011
[7] Hosoi, Y. Arao, H. Karasawa, H. Kawada. High-cycle fatigue characteristics of quasi-isotropic CFRP laminates, *Adv. Comp. Mater*., Vol 16, No. 2, 2007
[8] Hosoi, Y. Arao, H. Kawada. Transverse crack growth behaviour considering freeedge effect in quasi-isotropic cfrp laminates under high-cycle fatigue loading, *Composites Science and Technology*, 69, pp. 1388-1393, 2009
[9] A. Hosoi, J. Shi, N. Sato, H. Kawada: Variations of fatigue damage growth in crossply and quasi-isotropic laminates under high-cycle fatigue loading, *Journal of Solid Mechanics and Materials Engineering*, 3, No. 2, 2009
[10] T.J. Adam, P. Horst, P. Lorsch, M. Sinapius. Experimental Investigation of VHCF of Polymer Composites: Two Alternative Approaches, *MP Materials Testing*, 54, 11-12, pp. 734-741, 2012
[11] T.J. Adam, P. Horst. Very High Cycle Fatigue of Fibre-Reinforced Composites – An Alternative Experimental Approach, *Proceedings of the 19th Int. Conference on Composite Materials* – ICCM19, Montréal , pp.5012-5021, 2013
[12] P.A. Smith, S.L. Ogin. On transverse matrix cracking in cross-ply laminates loaded in simple bending, *Composites: Part A*, 30, pp.1003-1008, 1999
[13] A. Schmitz, P. Horst. A finite element unit-cell method for homogenized mechanical properties of heterogeneous plates, *Composites: Part A*, 61, pp. 23-32, 2014